Detection of acoustic oscillations of single gold nanospheres by time-resolved interferometry

Dijk, M.A. van; Lippitz, M.O.; Orrit, M.A.G.J.

Detection of Acoustic Oscillations of Single Gold Nanospheres by Time-Resolved Interferometry

Meindert A. van Dijk, Markus Lippitz, and Michel Orrit*

MoNOS, Huygens Laboratory, Universiteit Leiden, P.O. Box 9504, 2300 RA Leiden, The Netherlands

(Received 18 May 2005; published 23 December 2005)

We measure the transient absorption of single gold particles with a common-path interferometer. The prompt electronic part of the signal provides images for diameters as small as 10 nm. Mechanical vibrations of single particles appear on a longer time scale (period of 16 ps for 50 nm diameter). They reveal the full heterogeneity of the ensemble, and the intrinsic damping of the vibration. We also observe a lower-frequency mode involving shear. Ultrafast pump-probe spectroscopy of individual particles opens new insight into mechanical properties of nanometer-sized objects.

DOI: 10.1103/PhysRevLett.95.267406 PACS numbers: 78.67.Bf, 07.60.Ly, 63.22.+m

The confinement of electrons and phonons causes the physical properties of nanometer-sized objects to depart from those of bulk solids [1]. One of the ambitions of nanoscience is to exploit these deviations to tailor the properties of nanoparticles through their sizes and shapes. The plasmon resonance of noble-metal (silver and gold) particles is a collective oscillation of the conduction electrons, which governs their strong interaction with light. The shift and broadening of the plasmon resonance with changes in size and shape remains an active research area [2–4]. A further strong motivation for optical studies of metal nanoparticles is their recently proposed use as labels for molecular biology [5].

Working with ensembles of nanoparticles entails a fundamental difficulty. The current preparation methods generate a distribution of particles with a significant dispersion of sizes and shapes, and with many possible configurations of defects. This problem can be solved by the isolation of *single* nanoparticles. A number of methods have recently been put forward to study them with near-field [6] and far-field optical microscopy [7]. Each single nanoparticle can be studied in detail, and extended statistics can then be accumulated over many individuals. Following one and the same particle gives access to environmental influences and unravels space and time heterogeneity. Here, we find different electronic and elastic components in the time-resolved response of single gold nanoparticles. Combining short laser pulses with the microscopy of single nano-objects (molecules [8], semiconductor [9], or metal particles) offers new insight into their optical and mechanical properties on their characteristic times, picoseconds and shorter.

When an ultrashort pump pulse excites a metal particle, the absorbed energy is first conveyed to the conduction electrons, which collide within some tens of femtoseconds through electron-electron interactions [2–4]. On a 1 ps time scale, the hot electrons thermalize with the lattice, and, still later (typically 10 ps for a 10 nm particle), the whole particle cools down to ambient temperature via heat diffusion. The sudden heating of the electron gas has mechanical effects. Just as a sharp rap causes a bell to ring, an optical excitation launches elastic oscillations, via two mechanisms: First, a short-lived transient arises from the initial surge in electronic temperature and Fermi pressure. This pressure burst is short but strong because of the low heat capacity of the electron gas [10]. Second, as the electronic energy is shared with lattice modes on a picosecond time scale, anharmonicity leads to thermal expansion. For large enough particles, both times are short compared to the period of elastic vibrations (3.3 ps for the breathing of a 10 nm diameter particle [3]).

The optical properties of the hot particle are also modified. The initial excitation spreads the electronic population around the Fermi level, thereby opening new relaxation channels and broadening the surface plasmon resonance [11]. The subsequent thermal expansion of the lattice reduces the electron density, bringing about a red-shift of the plasmon resonance. Size variations can thus be optically detected via shifts of the plasmon resonance.

Laser-induced acoustic vibrations of nanoparticles have been previously studied on ensembles [3,4]. Such bulk observations are possible only as long as the oscillations are synchronized. Small differences in particle size within the ensemble lead to slight differences in oscillation periods. This inhomogeneous broadening, which often dominates the observed decay of the ensemble oscillation, is completely eliminated in our present study of single gold nanoparticles by interferometric pump-probe spectroscopy.

As a single nanoparticle is much smaller than the diffraction-limited laser spot, and as time-dependent changes in optical properties are small, the signals are weak. Measuring minute absorption changes requires many photons and the reduction of all noise sources, down to photon noise. An interferometer set close to its dark fringe suppresses intensity fluctuations on all time scales. We designed a common-path interferometer, in which two interfering pulses follow the same optical path at different times and with orthogonal polarizations (Fig. 1). Defects of the optical components (particularly

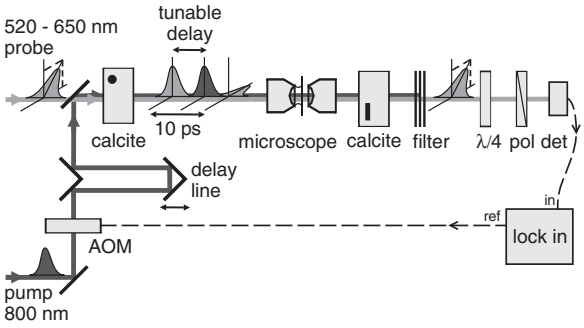

FIG. 1. Sketch of the pump-probe interferometer. A pump pulse and a pair of reference and probe pulses are focused on the sample in a microscope. The reference-probe pulses arise from a single pulse, split in time (10 ps delay) and polarization by a properly oriented calcite crystal. The delay between the pump pulse and the reference-probe pair can be scanned with a delay line. After the microscope, probe and reference are recombined by a second crystal, and their interference monitors pump-induced changes in the optical properties of the sample. A quarter-wave plate ($\lambda/4$) and a polarizer (pol) are used to set the working point of the interferometer.

of the objectives), being nearly identical for both polarizations, cancel to a large extent.

The measuring light pulse is linearly polarized at 45° from vertical and split into probe and reference pulses by a first birefringent crystal (calcite). The reference pulse is polarized along the crystal's horizontal fast axis, and the probe along the vertical slow axis. The pump pulse, being polarized along one of the crystal axes, is not split, and travels at a variable delay from the reference-probe pulse pair. After passage through the microscope, reference and probe pulses are recombined in a second, identical calcite crystal, with its fast axis vertical. Crystals as splitting elements have the advantage that alignment is easy, but the time delay (10 ps) is fixed by their thickness.

A pump-induced change in the real or imaginary part of the particle's dielectric permittivity causes a small variation $\Delta\zeta$ in the probe field's complex amplitude, from E to $(1 + \Delta\zeta)E$. This change is detected by the interferometer, either as an amplitude or as a phase variation. The working point of the interferometer is adjusted by independently rotating a quarter-wave plate and a polarizer. The amplitude-sensitive working point is obtained for slightly different amplitudes but equal phases of the interfering waves, and gives the variations of the real part $\mathrm{Re}(\Delta\zeta)$ of the probe field. At the phase-sensitive working point, the amplitudes are equal and the phases are slightly different, giving $\mathrm{Im}(\Delta\zeta)$. In the following, unless mentioned, we use the amplitude-sensitive working point.

The Fourier-limited 1 ps probe pulses are generated at a 76 MHz rate by an intracavity frequency-doubled optical parametric oscillator (OPO), tunable between 520 and 650 nm. The OPO itself is pumped at 800 nm by the 1 ps pulses of a Ti:sapphire laser. A small fraction of the latter beam, used as a pump, is modulated at 400 kHz by an acousto-optical modulator (AOM). The probe (and reference) power varied between 12 and 330 μW, the pump power between 0.5 and 5 mW. The homebuilt microscope includes an oil-immersion objective (numerical aperture NA = 1.4), and an air-spaced objective (NA = 0.95). The measurement spot has 300 nm diameter. The sample cover slide, mounted on a piezostage, can be scanned with 25 nm precision. The interferometer output is fed to an analog avalanche photodiode and demodulated in a lock-in amplifier.

The samples are roughly spherical gold particles with diameters ranging between 10 and 80 nm (British Biocell International and Sigma-Aldrich), spin coated with a poly(vinyl alcohol) solution (10 g/l) on a clean glass cover slide. The polymer film was about 20 nm thick.

Figure 2 shows images of single gold nanoparticles with 10 and 20 nm diameter. The preparation procedure was that of our earlier study [12], where third-harmonic signals proved that the particles were isolated. Figure 2 is recorded for zero delay, i.e., when the pump and probe pulses impinge simultaneously on the sample, providing maximum contrast. We extracted histograms from a set of images [12]. The discrimination threshold between noise and particles was $\mathrm{Re}(\Delta\zeta) = 2.7 \times 10^{-4}$ 2(b) and 1.3×10^{-4} 2(d). The resulting distributions, shown in Fig. 2(b) and 2(d), being monomodal and well separated from the background, confirm that each spot corresponds to a single particle. The relative width of the 20 nm distribution, 34%, is considerably larger than expected from the volume spread given by the manufacturer (19%). Additional fluctuations in shape, orientation, and surroundings of the particles can contribute to this large dispersion via shifts and intensity changes of the plasmon

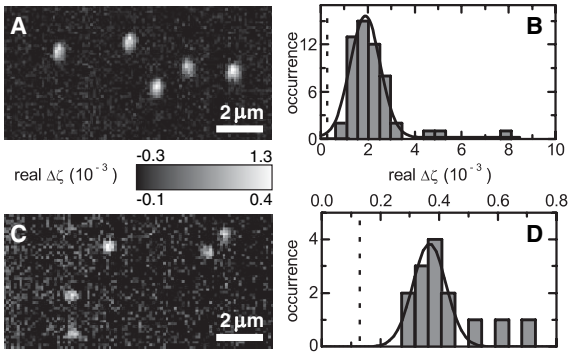

FIG. 2. Raster-scanned images of single gold nanoparticles and corresponding histograms of field changes $\mathrm{Re}(\Delta\zeta)$ for 20 nm (a),(b) and 10 nm diameter (c),(d). The integration times were 100 and 200 ms/pixel, respectively. A minimum signal level was required to start the fit to a Gaussian spot, indicated by a dashed line in the histograms. The relative width of the distributions, as deduced from rough Gaussian fits, is 34% (20 nm) and 11% (10 nm). The noise level in (c) is 7.1×10^{-5}, less than 3 times the shot-noise limit.

resonance, as recently observed by Berciaud *et al.* [13]. In order to minimize the spread in signal, we recorded the data of Fig. 2 with an off-resonant probe (635 nm).

By scanning the delay between the pump and the reference-probe pair, we monitor the time-resolved properties of the gold particles. Figure 3(a) shows a typical delay scan. The prompt response consists of two peaks, separated by 10 ps, with opposite signs because of the interferometric difference. The two peaks arise when the pump coincides with the reference and probe pulses, respectively, and are due to the broadening of the plasmon resonance by the pump pulse. On a longer time scale, reference and probe sample a damped oscillation in a differential way. From its frequency, we assign this oscillation to the fundamental acoustical breathing mode of a spherical particle (this purely radial mode has no angular dependence, and no node along the radius). The oscillations with the probe tuned to the red (595 nm) or to the blue (520 nm) of the particle's resonance are out of phase, which clearly shows that the signal mainly stems from a periodic shift of the plasmon resonance, as seen earlier in bulk experiments on silver nanoparticles [14].

By rotating the quarter-wave plate and the polarizer, we can set the interferometer to measure either purely absorptive or purely dispersive effects. This attractive feature provides both the real and imaginary parts of the *a priori* unknown optical response $\Delta\zeta$, without any need for a model or for previous knowledge. We measured delay scans for the same particle, with the interferometer set first at the amplitude-sensitive then at the phase-sensitive working points. From the measured interferometer outputs, we plotted the full $\Delta\zeta$ trace in the complex plane [Fig. 3(b)]. We again distinguish the two contributions discussed above. The fast component due to transient electronic heating is mainly dispersive at the chosen wavelength (520 nm). The second, slow one, originating from acoustic vibrations and indicated with the double arrow, is roughly perpendicular to the first part, and therefore dominantly absorptive at 520 nm. The different orientations of these components in the complex plane illustrate their different origins, as borne out by numerical simulations.

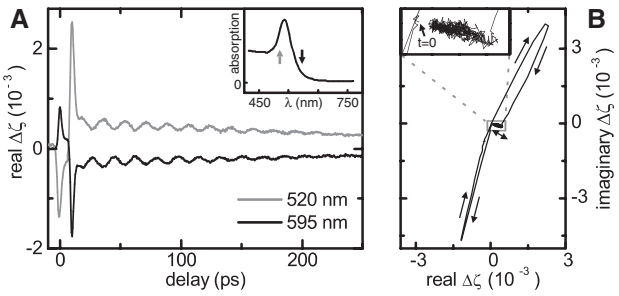

FIG. 3. (a) Two delay scans of one single gold particle, with the probe on the red side (black trace) and on the blue side (gray trace) of the surface plasmon resonance (see inset). The period of the oscillations is 17.6 ps for both traces, corresponding to a particle size of 53 nm [3]. (b) Full complex modification of the field by the particle, calculated from two traces with the interferometer set to either pure amplitude or pure phase sensitivity ($\lambda = 520$ nm). The arrows indicate the temporal progression. The inset shows a 7× zoom of the center part of the plot.

Because of their size and shape distribution, individual particles present slightly different oscillation periods, and they run out of phase on longer time scales [15]. This inhomogeneous broadening of the breathing mode totally masks any intrinsic damping of the ensemble oscillation. Selecting a single particle provides direct access to the intrinsic (or homogeneous) damping, by removing ensemble averaging. The damping rate is found to vary from particle to particle, probably through fluctuations of the environment and of the coupling to acoustic phonons in the substrate. The resonance quality factors $Q = \nu/\Delta\nu$ ($\Delta\nu$ being the mode's FWHM in the power spectrum) are about 4–5 for an ensemble, but reach considerably larger values, distributed between 15 and 30 (corresponding to amplitude $1/e$ relaxation times of 75–150 ps), for individual particles in the thin polymer film.

The elastic vibration modes of a solid sphere are labeled in Lamb's theory [16] by two integers, n, the harmonic order, i.e., the number of radial nodes, and l, the angular momentum number, which represents the angular dependence of the mode. We calculated the mode frequencies using bulk gold transversal and longitudinal sound velocities [17] following the equations given in Ref. [16] for free boundary conditions. Most of the particles show only the radial breathing mode $(n, l) = (0, 0)$ at a frequency $\Omega_{0,0}$, sometimes with a weak trace of the higher harmonic $(n, l) = (1, 0)$ at about $2.1\Omega_{0,0}$, as seen in ensemble measurements for silver nanoparticles [18]. Some particles, however, show an additional mode at a lower frequency. Figure 4(a) shows an example, where the time response

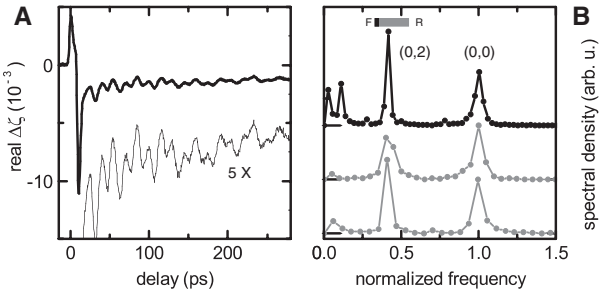

FIG. 4. (a) Delay scan of a single gold nanoparticle. The oscillation pattern shows a complex modulation. (b) Power spectra of this particle's oscillation (top spectrum) and of two other particles. Frequencies and amplitudes are normalized to those of the (0, 0) mode (the absolute frequencies were 67, 59, and 63 GHz, from top to bottom). The low-frequency peak (top spectrum: 28 GHz) lies between calculated frequencies of the (0, 2) mode for free boundary (F, thick line on bar) and for rigid boundary (R, end of bar). The ratio of its frequency to that of the breathing mode is constant.

clearly deviates from a sine curve. The power spectrum obtained by Fourier transformation of the oscillation [Fig. 4(b), top trace] shows two distinct peaks. The high-frequency peak (at 67 GHz for the upper spectrum) corresponds to the spherical breathing mode $(n, l) = (0, 0)$ of a 45 nm diameter gold sphere [3]. Another peak appears at lower frequency (28 GHz for the upper spectrum). This new peak cannot arise from the breathing mode of a second, larger particle at the same spot, for the optical signal (which scales as the third power of particle diameter) would then be too weak. We assign the peak at 28 GHz to the nonspherically symmetric $(n, l) = (0, 2)$ mode, involving shear strain (uniaxial cigar-to-pancake deformations of the sphere), which was seen already in Raman spectra of semiconductor nanoparticles [16]. We rule out the lower-order $(n, l) = (0, 1)$ mode, corresponding to a pear-shaped deformation, because it does not couple to the optical response, at least at the lowest order and in a spherically symmetric environment. Both modes can be excited by the isotropic heat pulse only if the spherical symmetry of the particle's expansion is broken either by the substrate or by the particle's shape. Indeed, the $(n, l) = (0, 2)$ mode does not appear in ensemble pump-probe experiments, where the particles' environment is isotropic. The measured frequency of the $(n, l) = (0, 2)$ mode lies between the frequencies expected for a sphere with free and rigid boundaries [see bar in Fig. 4(b)]. The shift from the free sphere's vibration could possibly arise from elastic perturbation by the glass half-space. We note, moreover, that the ratio of $(0, 2)$ to $(0, 0)$ frequencies was the same for all measured particles, which rules out deviations from the spherical shape as origin of the low-frequency mode, as these would vary from particle to particle.

Interferometric pump-probe measurements of single metal particles have the double advantage of high sensitivity and of providing the full optical response, including phase and amplitude. We have imaged 10 nm particles with 1 ps pulses, but shorter pulses would give access to even smaller particles, because of the improved time resolution and of the general enhancement of the nonlinear pump-probe signal by short pulses. Electronic properties such as scattering times could then be studied on a single-particle basis. On a longer time scale, we recorded time traces of acoustical breathing modes, displaying particle-to-particle fluctuations in frequency and decay rate, and revealing the intrinsic damping of mechanical vibrations. We found a new mode at lower frequency, so far unobserved in pump-probe experiments and presumably coupled by a substrate-induced breaking of the spherical symmetry. Mechanical vibration modes are fascinating doorways to the elastic properties of metal particles and of their environment. More generally, probing single nano-objects and nanostructures with short laser pulses opens a wealth of real-time studies of nanomechanics on picoseconds, the characteristic vibration times at nanometer length scales.

M. L. acknowledges a Marie Curie grant from the European Commission (Contract No. HPMF-CT-2002-02099). This work is part of the research program of the ''Stichting voor Fundamenteel Onderzoek der Materie'' (FOM), financially supported by the NWO.

*Corresponding author.
Electronic address: orrit@molphys.leidenuniv.nl

[1] U. Kreibig and M. Vollmer, *Optical Properties of Metal Clusters*, Springer Series in Materials Science Vol. 25 (Springer, Berlin, 1995).
[2] S. Link and M. A. El-Sayed, J. Phys. Chem. B **103**, 8410 (1999).
[3] G. V. Hartland, Phys. Chem. Chem. Phys. **6**, 5263 (2004).
[4] C. Voisin *et al.*, J. Phys. Chem. B **105**, 2264 (2001).
[5] S. Schultz *et al.*, Proc. Natl. Acad. Sci. U.S.A. **97**, 996 (2000); L. Cognet *et al.*, Proc. Natl. Acad. Sci. U.S.A. **100**, 11 350 (2003); G. Raschke *et al.*, Nano Lett. **3**, 935 (2003); C. D. Geddes, A. Parfenov, and J. R. Lakowicz, J. Fluoresc. **13**, 297 (2003).
[6] G. P Wiederrecht, Eur. Phys. J. Appl. Phys. **28**, 3 (2004).
[7] M. A. van Dijk, M. Lippitz, and M. Orrit, Acc. Chem. Res. **38**, 594 (2005).
[8] E. M. H. P. van Dijk *et al.*, Phys. Rev. Lett. **94**, 078302 (2005).
[9] T. Guenther *et al.*, Phys. Rev. Lett. **89**, 057401 (2002).
[10] M. Perner *et al.*, Phys. Rev. Lett. **85**, 792 (2000).
[11] M. Perner *et al.*, Phys. Rev. Lett. **78**, 2192 (1997).
[12] M. Lippitz, M. A. van Dijk, and M. Orrit, Nano Lett. **5**, 799 (2005).
[13] S. Berciaud *et al.*, Nano Lett. **5**, 515 (2005).
[14] N. Del Fatti *et al.*, J. Phys. Chem. A **104**, 4321 (2000).
[15] See EPAPS Document No. E-PRLTAO-96-024602 for a direct comparison of single-particle measurements to an ensemble measurement. This document can be reached via a direct link in the online article's HTML reference section or via the EPAPS homepage (http://www.aip.org/pubservs/epaps.html).
[16] L. Saviot *et al.*, J. Non-Cryst. Solids **197**, 238 (1996).
[17] C. Voisin *et al.*, Physica (Amsterdam) **316B**, 89 (2002).
[18] A. Nelet *et al.*, Appl. Surf. Sci. **226**, 209 (2004).